

## 荧光介孔二氧化硅纳米粒子的合成及药物运输

陈敏敏<sup>#,1,2</sup> 耿浩然<sup>#,1</sup> 胡金霞<sup>1,2</sup> 张 琼<sup>3</sup>

Godfred Amfo Agyekum<sup>3</sup> 张卓琦<sup>\*,3</sup> 曹希传<sup>\*,1</sup>

(<sup>1</sup> 中国矿业大学材料科学与工程学院, 徐州 221000)

(<sup>2</sup> 中国矿业大学化工学院, 徐州 221000)

(<sup>3</sup> 徐州医科大学附属医院心内科, 徐州 221000)

**摘要:** 合成了荧光介孔二氧化硅纳米粒子(MSNs-FITC),并研究了其在持续药物释放和生物示踪成像方面的应用。首先,采用一步法合成出 MSNs-FITC,结合 SEM、TEM、FT-IR、XRD 和氮气吸附脱附等表征技术进行表征。其次,将抗癌药物阿霉素(DOX)负载到 MSNs-FITC 中。载药粒子的药物释放行为具有明显的 pH 依赖性,酸性环境加速释放速率。同时,体外细胞毒性测试表明 MSNs-FITC 具有良好的生物相容性。激光共聚焦扫描显微镜(CLSM)图像表明,MSNs-FITC 可以进入细胞并具有剂量依赖性,流式细胞术分析(FCM)进一步证明了这一结果。

**关键词:** 介孔二氧化硅纳米载体; 药物运输; 细胞毒性; 生物成像

中图分类号: O613.72 文献标识码: A 文章编号: 1001-4861(2019)11-2125-11

DOI: 10.11862/CJIC.2019.244

## Synthesis of Fluorescent Mesoporous Silica Nanoparticles and Application for Intracellular Drug Delivery

CHEN Min-Min<sup>#,1,2</sup> GENG Hao-Ran<sup>#,1</sup> HU Jin-Xia<sup>1,2</sup> ZHANG Qiong<sup>3</sup>

Godfred Amfo Agyekum<sup>3</sup> ZHANG Zhuo-Qi<sup>\*,3</sup> CAO Xi-Chuan<sup>\*,1</sup>

(<sup>1</sup>School of Materials Science and Engineering, China University of Mining and Technology, Xuzhou, Jiangsu 221000, China)

(<sup>2</sup>School of Chemical Engineering and Technology, China University of Mining and Technology, Xuzhou, Jiangsu 221000, China)

(<sup>3</sup>Department of Cardiology, the Affiliated Hospital of Xuzhou Medical University, Xuzhou, Jiangsu 221000, China)

**Abstract:** Here, we reported the synthesis and FITC-functionalized of mesoporous silica nanoparticles (MSNs) for tracing bioimaging and sustained drug release. Firstly, the MSNs-FITC were synthesized through one-pot method and characterized by SEM, TEM, FT-IR, XRD and the N<sub>2</sub> adsorption-desorption isotherm respectively. Then a classic anticancer drug doxorubicin (DOX) was loaded into the MSNs-FITC. The DOX-loaded nanocarriers exhibited obviously pH dependent release behavior with accelerated release rate in acidic environment. Meanwhile, the in vitro cytotoxicity evaluation exhibited that the nude MSNs-FITC were highly biocompatible. Furthermore, the confocal laser scanning microscope (CLSM) images indicated that MSNs-FITC could penetrate into living cells effectively and dose-dependent internalization of MSNs-FITC were further investigated by flow cytometry analysis (FCM).

**Keywords:** mesoporous silica nanocarriers; drug delivery; cytotoxicity; bioimaging

收稿日期: 2019-08-13。收修改稿日期: 2019-10-04。

中央高校基本科研业务费专项资金(No.2018BSCXB11)和江苏省研究生科研与实践创新计划项目(No.KYCX18\_1937)资助。

<sup>#</sup> 共同第一作者。

\*通信联系人。E-mail: zhuoqizhang@sina.com, xichuancao@cumt.edu.cn

## 0 Introduction

Cancer remains a major cause of death in most countries in the world and the incidence of cancer increases with age<sup>[1]</sup>. To achieve the efficacy, the traditional chemo-therapy requires high doses of cancer drug reaching the tumor site through the blood circulation. For one thing, the drug utilization is very low, for another, high cytotoxicity of the drug always causes serious side effects in the normal tissue site. Thus, ideal drug delivery systems (DDSs) are sought much needed. As one of the DDSs to treat cancer, nanotherapeutic systems can protect the drug from releasing prematurely. In addition, they have other unique advantages: increased stability of anti-cancer drugs in blood, decreased non-specific toxicity, and easy modification of particle surface for targeting systems<sup>[2-4]</sup>. To date, plentiful nanotherapeutic systems have been developed and exemplified regarding traditional systems such as liposomes<sup>[5-6]</sup>, polymer-based therapeutics<sup>[7-8]</sup>, carbon nanotubes<sup>[9]</sup>, and silica particles<sup>[10-11]</sup> etc.

Since Vallet-Regí et al.<sup>[12]</sup> firstly reported MCM-41 mesoporous silica as drug carrier of ibuprofen for controlled release in the year of 2001, mesoporous silica nanoparticles (MSNs) have opened up new and exciting possibilities in the field of cancer cure<sup>[13-17]</sup>. Silica has been approved by the United State Food and Drug Administration (US FDA) as “Generally Recognised As Safe” and by the European Union (EU) for its use in cosmetics and food additives<sup>[18]</sup>. In particular, the applications of MSNs in drug delivery have been intensively focused. MSNs possess several attractive features such as large surface area with abundant activity of Si-OH, which could easily immobilize various functional materials in the external surface of the MSNs before surfactant removal to generate multifunctional nanomedical platforms for multimodal imaging or simultaneous diagnosis and therapy<sup>[19-21]</sup>. On the other hand, mesoporous silica nanoparticles are solid materials which are comprised of a honeycomb-like rigid porous structure with hundreds of empty channels (mesopores) that are able

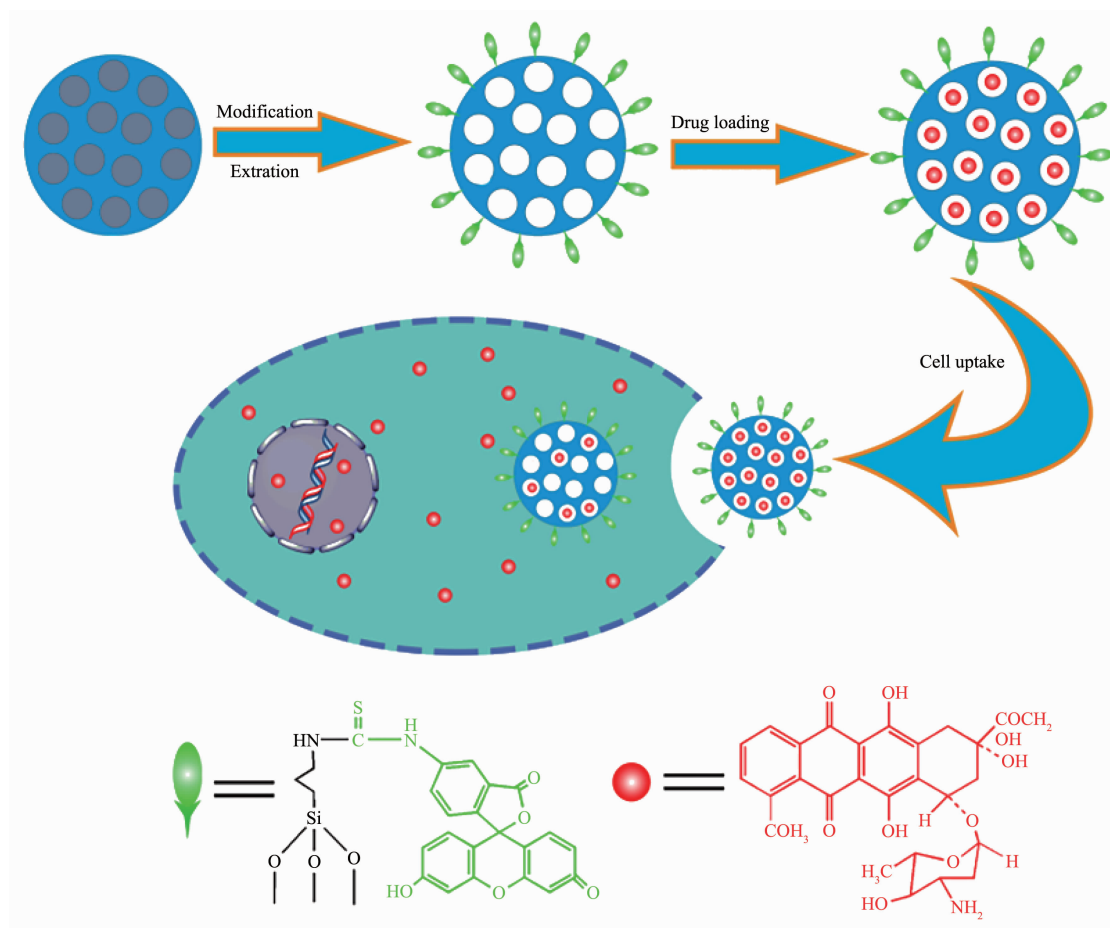
to absorb/encapsulate relatively large amounts of therapy drug molecules under mild conditions. Furthermore, the MSNs also have the ability to effectively protect the entrapped molecules from premature release and degradation due to their excellent bio-stability under physiological conditions<sup>[22]</sup>. As a result of their excellent biocompatibility, modifiable external surface with abundant Si-OH, large surface area, high pore volume, and adjustable pore size, MSNs are developed to be one of the most important candidates for drug carriers<sup>[23-27]</sup>.

In this contribution, MSNs functionalized orderly with amino groups and FITC were prepared as shown in Scheme 1. The weak base type drug doxorubicin (DOX), a classic anticancer drug in clinic, was used as the model drug to assess the drug loading and releasing behaviors of the carriers. The in vitro cellular cytotoxicity test was performed to evaluate the biocompatibility of MSNs-FITC, and the cytotoxic effect of DOX@MSNs-FITC to Hela cells was also investigated. Cell uptake of MSNs was monitored by CLSM and Flow Cytometry (FCM). The results reported here support the potential of amino-functionalized MSNs as a nanocarrier for simultaneous controlled drug release based on the low pH value in cancer/tumors and fluorescent bioimaging.

## 1 Experimental

### 1.1 Materials

Cetyltrimethyl ammonium chloride (CTAC, 98%), tetraethylorthosilicate (TEOS, 99%), and diethanolamine (DEA, 98%) were obtained from Shanghai Chemical Reagents Company (Shanghai, China). Doxorubicin (DOX) and [3-(2-aminoethyl)aminopropyl] trimethoxysilane (APTES) were purchased from Sigma-Aldrich (America). Fluorescein isothiocyanate (FITC) was purchased from Alfa Aesar (America). Hela cells were obtained from Chinese Academy of Sciences Cells Bank (Shanghai, China). Phosphate-buffered saline (PBS), 3-(4,5-dimethylthiazol-2-yl)-2,5-diphenyltetrazolium bromide (MTT) and 2-(4-amidinophenyl)-6-indolecarbamidine dihydrochloride (DAPI) were purchased from Beyotime (Shanghai, China). Dulbeccos modified



Scheme 1 Schematic illustration for the preparation of MSNs-FITC and cell uptake

Eagle medium (DMEM), fetal bovine serum (FBS), penicillin-streptomycin solution and Trypsin-EDTA solution were obtained from Gibco (America). All the chemicals were of analytical grade and used without further treatment. All solutions were prepared and diluted using ultrapure water from the Millipore Milli-Q system.

## 1.2 Characterization

The morphology and structure of MSNs samples were characterized via transmission electron microscopy (TEM) and scanning electron microscope (SEM). TEM micrographs were obtained on a FEI Tecnai G2S-Twin microscope with a field emission gun operating at 200 kV. SEM micrographs were obtained on a JEOL JSM-6700F microscope with acceleration voltage of 10 kV. Powder X-ray diffraction (XRD) patterns were recorded on a Rigaku D/Max 2550 X-ray diffractometer with Cu  $K\alpha$  radiation (40 kV, 20 mA) at  $\lambda=0.15418$  nm with a scanning rate of  $1^\circ \cdot \text{min}^{-1}$  over a range of  $0.8^\circ \sim$

$6.0^\circ$  ( $2\theta$ ) with a step width of  $0.02^\circ$ . The pore characteristics of the samples were studied by determining the nitrogen adsorption using a Micromeritics ASAP 2020M system. Their surface area was calculated by the Brunauer-Emmett-Teller (BET) approach and the pore size distributions were obtained by the Barrett-Joyner-Halenda (BJH) method. FTIR measurement was recorded on a Bruker IFS 66V/S FTIR spectrometer using KBr pellets as background. UV-Vis absorption spectra were performed using a Thermo EV-60 spectrophotometer in the range between 1 000 and 300 nm. Intracellular tracking was subjected to be observed with FV1000 confocal laser scanning microscopy. Transfer capability was recorded by BD FACS Calibur Flow cytometry.

## 1.3 Synthesis of mesoporous silica nanoparticles (MSNs)

MSNs were synthesized with the sol-gel method. The following is a typical synthesis example: 6.4 mL

water (0.36 mol), 0.9 g ethanol (0.015 mol), 1.04 g of a 25%(w/w) CTAC solution (0.786 mmol), and 0.02 g DEA (0.19 mmol) were mixed and stirred vigorously at 40 °C for 30 min. Then 0.73 mL TEOS (3.25 mmol) was added dropwise into the above solution within 2 min and the mixture was continuously under stirring for another 2 h. Finally, with the resulting white solution being cooled to room temperature, the particles (denoted as CTAC/MSNs) were collected by centrifugation and washed several times by water and methanol alternately. The surfactant CTAC was then removed by reflux in a mixture of 70 mL methanol and 0.70 mL concentrated 37.2%(w/w) HCl at 80 °C for 6 h. The resulting particles (denoted as MSNs) were then collected in the same way as CTAC/MSNs.

#### 1.4 Synthesis of fluorescent MSNs-FITC

A typical synthesis procedure was depicted as following: 1 mg FITC was reacted with 5  $\mu$ L APTES in 1 mL absolute ethanol by stirring for 24 h in darkness at room temperature to obtain the FITC-conjugated APTES (APTES-FITC). Then 20  $\mu$ L APTES-FITC was mixed with the as-synthesized CTAC/MSNs for further 2 h stirring in darkness at 40 °C. The solution was cooled to room temperature and collected by centrifugation (denoted as CTAC/MSNs-FITC). Similarly, the surfactant-free particles (denoted as MSNs-FITC) were obtained by extraction as mentioned above.

#### 1.5 Loading and release of DOX

DOX was used as a model drug molecules agent to evaluate the drug loading and releasing manner. Typically, 4 mg MSNs-FITC were immersed in 4 mL buffered solution at pH of 7.4 containing 560  $\mu$ g DOX. After stirring for 24 h under light-sealed conditions, the mixture was centrifuged and the supernatant was removed. The DOX@MSNs-FITC were obtained and washed twice with PBS solution to wash away the DOX adsorbed on the external surface. The supernatant solution concentration was calculated based on absorbance intensity at 483 nm via UV-Vis spectroscopy (Thermo EV-60, American). DOX loading capacity ( $C_{\text{load}}$ ) and entrapment efficiency ( $\eta_{\text{entrapment}}$ ) in the nanoparticles were calculated by the following

equations:

$$C_{\text{load}} = \frac{M_{\text{load}}}{M_{\text{nanoparticles}}} \times 100\%$$

$$\eta_{\text{entrapment}} = \frac{M_{\text{load}}}{M_{\text{feed}}} \times 100\%$$

Where  $M_{\text{load}}$  is the mass of DOX loaded into nanoparticles (mg),  $M_{\text{nanoparticles}}$  is the mass of nanoparticles (g),  $M_{\text{feed}}$  is the mass of DOX in feed (mg).

The release kinetics of DOX from DOX@MSNs-FITC were carried out in phosphate buffered saline (PBS) at 37 °C and shaken at 120 r·min<sup>-1</sup>. 4 mg DOX@MSNs-FITC were dispersed in 4 mL PBS (pH=7.4, 5.5, and 4.6, respectively), followed by 1 mL of solution collected at timed intervals. The volume of the release medium kept constant by adding 1 mL fresh medium after each sampling. The released DOX was analyzed by UV-Vis. The releasing efficiency ( $\eta_{\text{release}}$ ) was calculated by the following equations:

$$\eta_{\text{release}} = \frac{M_{\text{release}}}{M_{\text{load}}} \times 100\%$$

Where  $M_{\text{release}}$  is the mass of DOX in the release medium (mg).

#### 1.6 Cell viability assay

Hela cells were cultured as a monolayer in DMEM medium supplemented with 10% (V/V) FBS at 37 °C in a humidified incubator (5%(V/V) CO<sub>2</sub> in air). The MTT assay was used to measure cell viability. Briefly, cells were seeded in 96-well plates at a density of 1×10<sup>4</sup> cells per well and four duplicate wells were set up in each sample. After incubation for 24 h at 37 °C in 100  $\mu$ L DMEM medium containing 10% FBS, culture medium was discarded and then cells were treated with free DOX, DOX@MSNs-FITC or blank MSNs-FITC at various concentrations. After incubation for 24 h, 20  $\mu$ L of MTT solution (5 mg·mL<sup>-1</sup>) was added to each well and the plate was incubated in the CO<sub>2</sub> incubator for an additional 4 h. The precipitated formazan violet crystals were dissolved in 150  $\mu$ L of DMSO. The optical density (OD) value of each individual well was calculated using a spectrophotometer (Thermo MK3, American) at 570 nm absorbance. With untreated cells in medium used as a control and corresponding groups without cells



used as blanks, all experiments were carried out with four replicates.

### 1.7 Confocal microscopy assay

The HeLa cells were seeded into 24-well plates at a density of  $3 \times 10^4$  cells per well respectively. After a 24 h incubation period, the cells were treated with MSNs-FITC at various concentrations for 4 h. Then culture medium was removed, cells were swashed with PBS three times. After the removal of supernatants, the cells were fixed with 4% ( $w/V$ ,  $g \cdot mL^{-1}$ ) paraformaldehyde for 30 min. Subsequently, the slides were rinsed with PBS three times and the cells were stained with DAPI for 10 min. Finally, the intracellular localizations of MSNs-FITC were directly visualized with CLSM. In the assay, all experiments were carried out under a light-sealed condition.

### 1.8 Flow cytometry analysis

FCM was used to demonstrate the transfer capability of the MSNs-FITC nanoparticles into cells. HeLa cells were seeded into a 6-well plate ( $5 \times 10^5$  cells per well), and cultured for 24 h, then treated with MSNs-FITC at various concentrations with the untreated cells used as blank control. After incubating for 4 h, the media was removed, and the cells were swashed twice with PBS buffer to remove residual nanoparticles. Then, with the cells being harvested with 0.25% ( $V/V$ ) trypsin solution, washed with PBS buffer three times, and finally suspended in PBS, the signals of FITC fluorescence were recorded by FCM. In the assay, all experiments were carried out under a light-sealed condition to avoid photo bleaching.

## 2 Results and discussion

### 2.1 Preparation and characterization

The MSNs were synthesized using a base-catalyzed sol-gel method with TEOS as the silica precursor, the CTAC surfactant as the template and Diethanolamine as the catalyst. The MSNs were then functionalized with FITC by one-pot procedure grafting to obtain the APTES-FITC functionalized MSNs. The size and pore structure of the MSNs-FITC were characterized by SEM, TEM, FT-IR and  $N_2$  adsorption-desorption test.

TEM image showed MSNs-FITC as rough spheres with an average size of approximately 150 nm in diameter (Fig.1A). The SEM image also showed that the spherical MSNs-FITC were well dispersed without any obvious aggregation (Fig.1B).

The pore structure of MSNs before and after the functionalization was examined using small-angle powder XRD. Both MSNs and MSNs-FITC showed two broad peaks which suggested short-range ordering and a wormlike pore structure inside the nanoparticles. It could be revealed that the fluorescence groups were functionalized on MSNs successfully as a result of the decrease in intensity and slight change in the position of the peaks.

In order to form mesoporous structure, CTAC surfactants in the pore had to be removed by extraction. In addition, the residual CTAC surfactants would bring cytotoxicity and decreased the biocompatibility of carriers. As shown in the FT-IR spectra of CTAC/MSNs (Fig.3A), owing to the large

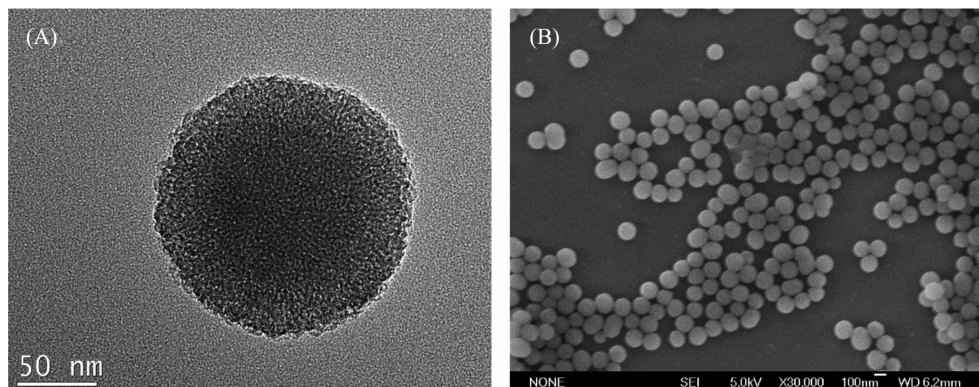


Fig.1 (A) TEM image of the synthesized MSNs-FITC and (B) SEM image of the synthesized MSNs-FITC

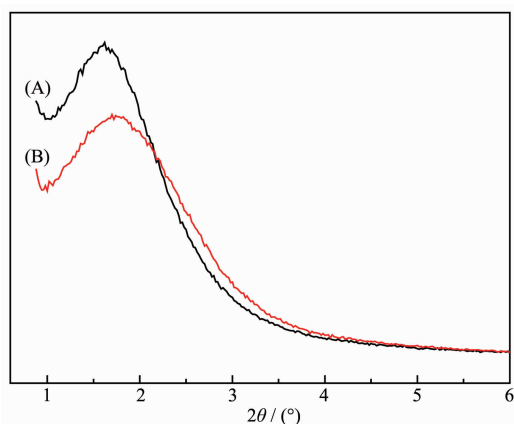


Fig.2 Small-angle XRD patterns of the (A) MSNs and (B) MSNs-FITC

amount of CTAC present in the channel, CTAC/MSNs gave the characteristic C-H stretching vibrations at  $2\,924$  and  $2\,854\text{ cm}^{-1}$ , and C-H deformation vibration around  $1\,478\text{ cm}^{-1}$  [28]. After removal of CTAC, these C-H peaks derived from CTAC disappeared, suggesting that the CTAC molecules had been removed successfully (Fig.3B). Peaks at  $3\,390$  and  $1\,635\text{ cm}^{-1}$  were assigned to H-O-H groups present on the surface of MSNs or due to water molecules adsorbed [29]. The peaks at  $1\,086$ ,  $801$  and  $463\text{ cm}^{-1}$  were all characteristic absorbance bands of silica, and corresponded to Si-O-Si asymmetric stretching, Si-O-Si symmetric stretching and Si-O-Si bending, respectively [30]. However, the MSNs-FITC showed the C-H bonds at  $2\,924$ ,  $2\,854$ ,  $1\,480\text{ cm}^{-1}$  again and C=O bonds at  $1\,728\text{ cm}^{-1}$  [31] after further grafting APTES-FITC (Fig.3C). Furthermore, a clear IR peak centered at  $1\,558\text{ cm}^{-1}$  appeared and

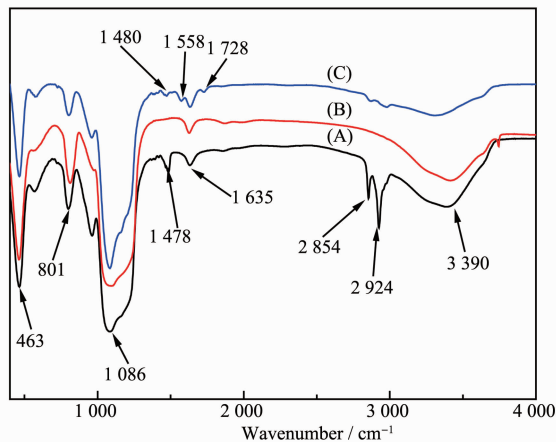
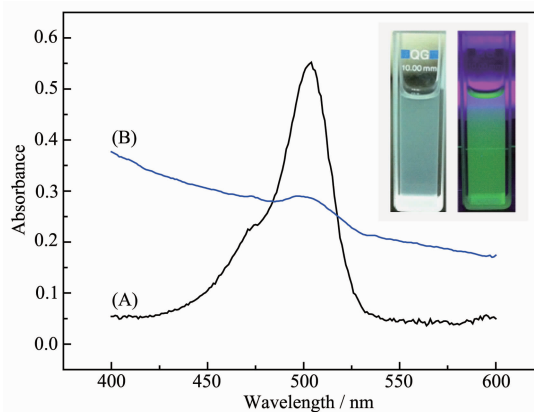


Fig.3 FT-IR spectra of (A) CTAC/MSNs, (B) MSNs and (C) MSNs-FITC

could be assigned to the N-H bonds [32], which revealed that the functionalization of fluorescence groups was successful.

To further verify the successful grafting of FITC on the MSNs, UV-Vis absorption spectroscopy was utilized as shown in Fig.4, which displayed that the successfully FITC-conjugated with APTES (APTES-FITC) in water exhibited the main absorption bands at  $496\text{ nm}$  (Fig.4A). This band was also present in the spectrum of MSNs-FITC (Fig.4B), indicating a successful conjugation of FITC on MSNs successfully, which also can be proved by the strong green fluorescence of MSNs-FITC irradiated with UV lamp (right), but no fluorescence irradiated with white lamp (left) in the inset photographs.



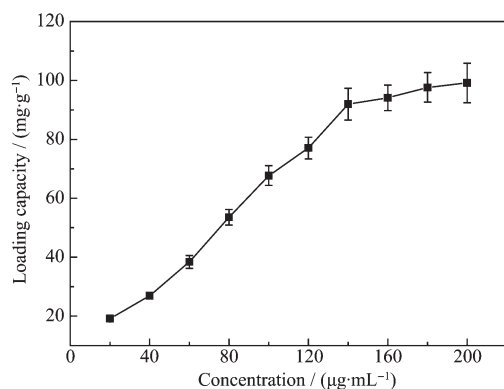
Insets are photographs of MSNs-FITC dispersed in PBS under white light (left), and MSNs-FITC dispersed in PBS under UV light (right) situations

Fig.4 UV-Vis absorption spectra of (A) APTES-FITC and (B) MSNs-FITC

## 2.2 Drug loading and *in vitro* release of DOX

To evaluate the drug loading capacity and releasing behaviour of MSNs-FITC, a classic water-soluble anticancer drug DOX was used as a model drug. The nanocarrier was loaded with DOX by soaking them in a concentrated drug-PBS solution at pH value of 7.4, then collected by centrifugation and washed with PBS several times. UV-Vis spectroscopy was used to determine the DOX loading capacity and release properties. As shown in Fig.5, the DOX was loaded in nanocarrier with different concentrations, the drug loading content increased along with the

increase of the DOX concentration. When the concentration was less than  $140 \mu\text{g} \cdot \text{mL}^{-1}$ , the drug loading content quickly increased, and DOX loading capacity and entrapment efficiency reached  $91.96 \text{ mg} \cdot \text{g}^{-1}$  ( $8.42\%(w/w)$ ) and  $65.7\%$  at the concentration of  $140 \mu\text{g} \cdot \text{mL}^{-1}$ . But it increased slowly once the concentration was between  $140$  and  $180 \mu\text{g} \cdot \text{mL}^{-1}$ . Moreover, with the concentration raising to  $180$  and  $200 \mu\text{g} \cdot \text{mL}^{-1}$ , the loading capacity hardly increased and approximately reached saturation, which demonstrated that the continuously increased concentration would not lead to increased encapsulation efficiency.

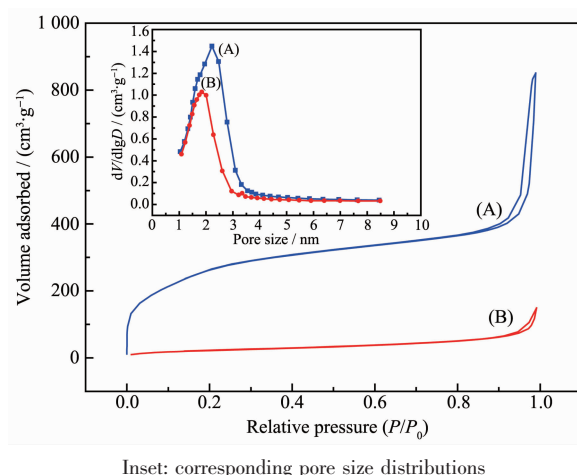


Results are expressed as mean  $\pm$  the standard error from three independent experiments

Fig.5 Loading capacity of MSNs-FITC in different DOX concentrations

To prove that the DOX molecules could penetrate into the hole of mesopores of the MSNs-FITC, BET analysis was also carried out as shown in Fig.6. The specific surface area and cumulative pore volume of the nude MSNs-FITC were calculated to be  $861 \text{ m}^2 \cdot \text{g}^{-1}$  and  $1.48 \text{ cm}^3 \cdot \text{g}^{-1}$ . However, after drug loading, the values of calculated specific surface area and cumulative pore volume of the materials decreased to about  $148 \text{ m}^2 \cdot \text{g}^{-1}$  and  $0.99 \text{ cm}^3 \cdot \text{g}^{-1}$ , respectively. Furthermore, the average pore size measured before and after the DOX loading were  $2.2$  and  $1.8 \text{ nm}$  respectively. As the results clearly indicated, the BET surface area, pore volume, and pore diameter of MSNs-FITC were all decreased significantly after the loading of DOX, suggesting the DOX molecules had penetrated into the nanopores.

The studies of DOX released from DOX@MSNs-

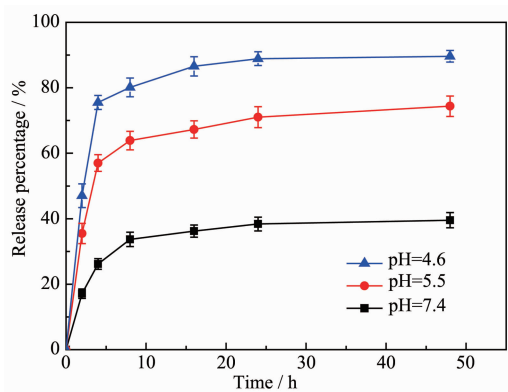


Inset: corresponding pore size distributions

Fig.6 Nitrogen adsorption-desorption isotherms of (A) MSNs-FITC and (B) DOX@MSNs-FITC

FITC were conducted under different PBS buffer solutions at pH values of  $7.4$ ,  $5.5$ , as well as  $4.6$  at  $37^\circ\text{C}$ . The *in vitro* cumulative drug release profiles over a period of  $48 \text{ h}$  were shown in Fig.7. The results demonstrated that the DOX release performance was obviously pH dependent and cumulative release amount increased with the decrease of pH. At pH value of  $7.4$ , the release amount was quite low and only approximately  $38\%(w/w)$  was released in  $24 \text{ h}$ . At pH value of  $5.5$ , the release amount gradually increased to  $71\%(w/w)$  in  $24 \text{ h}$  and exhibited relatively faster release rate. Subsequently, when pH value decreased to  $4.6$ , a faster release behavior was obtained and the release amount reached  $89\%(w/w)$  in  $24 \text{ h}$ . This is because the drug release was mainly determined by the effect of electrostatic interaction between DOX molecules and the nanoparticles surface. It is known that the  $\text{pK}_a$  of DOX is  $8.3$  adjacently, so most amine groups of DOX exist as protonated forms ( $-\text{NH}_3^+$  forms) in the range of pH values examined here [33]. On the other hand, the  $\text{pK}_a$  of Si-OH on the internal surface of MSNs ranged from  $4$  to  $5$ . It means that the higher the pH value of the medium was, the more negative charges were on the internal surface of the mesopores, the stronger attraction existed between the positively charged DOX and the negatively charged carriers, so the more difficult for the loaded DOX to be released out of the nanoparticles [34-35]. It is well documented that pH values in different tissues

and cellular compartments vary significantly. For example, the tumor extracellular environment is more acidic (pH=6.8) than blood and normal tissues (pH=7.4), and the pH values of late endosome and lysosome are even lower, at 5.0~5.5<sup>[36-37]</sup>. So the sustained release properties are favorable for increased drug accumulation in the cytoplasm of cancer cells following endocytosis and reduced drug release from the carriers in normal tissue, and can thus enhance the long-term chemotherapy efficacy and reduce non-specificity toxicity.



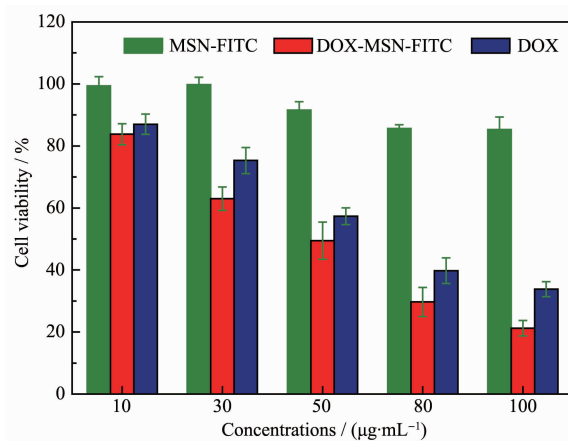
Results are expressed as mean  $\pm$  the standard error from three independent experiments

Fig.7 *In vitro* DOX release profiles from MSNs-FITC at different pH values

### 2.3 *In vitro* cell cytotoxicity assay and cell uptake

An efficient drug delivery system should not only have sustained release properties, but also possess favorable biocompatibility. The *in vitro* cytotoxicity in Hela cells was investigated by MTT assay as shown in Fig.8. The blank MSNs-FITC had a negligible cytotoxicity after being cultured with Hela cells for 24 h, even at concentrations as high as 100  $\mu\text{g}\cdot\text{mL}^{-1}$ . The well biocompatible on Hela cells could be attributed to the relatively low concentration of the surfactants in MSNs-FITC. To further demonstrate the pharmacological activity of the DOX@MSNs-FITC, their cytotoxic effects were also tested. Conversely, when the Hela cells were treated with either free DOX solution or the suspension of DOX@MSNs-FITC with equal DOX dosage, the result exhibited increased cytotoxicity with the increase of the concentration of the DOX. But DOX@MSNs-FITC showed stronger effect on killing

tumor cells than free DOX at the same dosage<sup>[38-39]</sup>. This may be because the carrier loading DOX is more biocompatible than the free DOX, so it can easily disguise as harmless substances to enter the cells by endocytosis. Once the carrier entered into the cytoplasm of the cell, it began to release the loading drug molecules due to the acidic surroundings thereby causing more cell death as a result of the high intracellular concentration of DOX. Free DOX will be excluded in the process of endocytosis thereby causing less cell death due to the low intracellular concentration of DOX. Therefore, it could be concluded that MSNs-FITC have been a promising potential candidate for drug loading and delivery in cancer therapy.

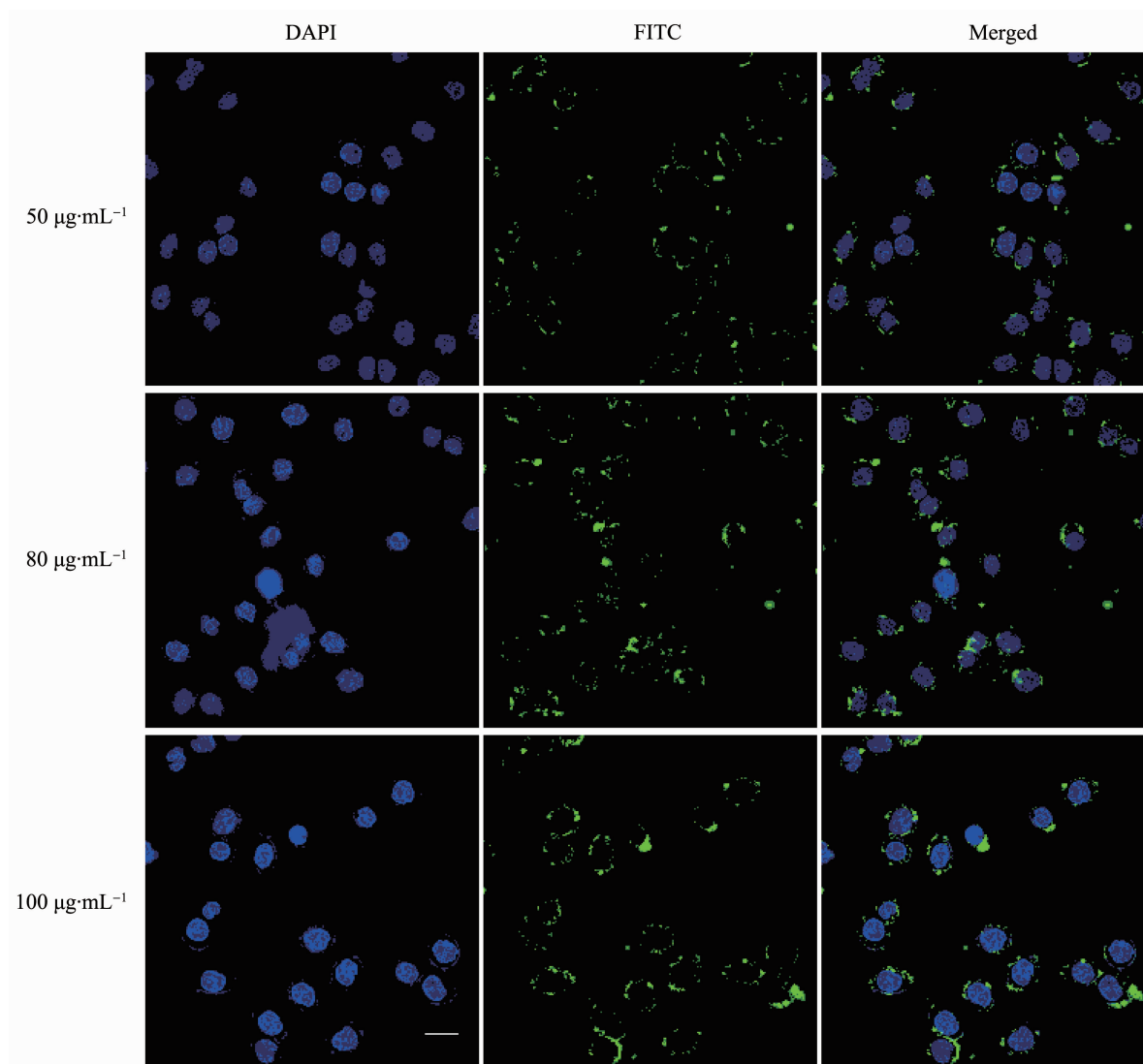


Results are expressed as means  $\pm$  the standard error from three independent experiments

Fig.8 Cytotoxicity of blank nanoparticles, free DOX and equivalent DOX concentration of DOX-loaded nanoparticles in Hela cells for 24 h

Effective endocytosis of the nanocarriers by cancer cell is a critical role for intracellular drug delivery. CLSM analysis was performed to examine the cellular endocytosis and sequential distribution of nanocarriers. Fig.9 showed the CLSM images of Hela cells cultivated with different MSNs-FITC concentrations at 50, 80 and 100  $\mu\text{g}\cdot\text{mL}^{-1}$ . To confirm the efficient uptake of the nanocarriers by cancer cells, different concentrations of MSNs-FITC were incubated with Hela cells in DMEM at 37  $^{\circ}\text{C}$  for 4 h. The blue regions represent the signal from the nucleus stained with DAPI, and the green regions are the signal from FITC. The green fluorescence could be observed





Blue fluorescence shows nuclei stained with DAPI. Green fluorescence shows the location of MSNs-FITC. The scale bar is 20  $\mu\text{m}$

Fig.9 Confocal laser scanning microscope images of HeLa cells cultivated with different concentrations of MSNs-FITC at 50, 80 and 100  $\mu\text{g}\cdot\text{mL}^{-1}$

clearly in almost all of the cells from the CLSM images and distributed around nucleus intensively, demonstrating that these nanocarriers could penetrate the plasma membrane of HeLa cells and transferred into the cytoplasm with high efficiency. Moreover, the intensity of green fluorescence could be obviously recognized after incubation at 100  $\mu\text{g}\cdot\text{mL}^{-1}$ , which was stronger than that incubated at 50  $\mu\text{g}\cdot\text{mL}^{-1}$ , suggesting the dose-dependent endocytosis by HeLa cells<sup>[40]</sup>. This evidence visually confirms that MSNs-FITC can be used as a transmembrane delivery carrier for potential drug delivery and as a fluorescent tracer for live cell imaging with realtime monitoring

properties.

Dose-depended internalization of MSNs-FITC was further investigated by FCM analysis. Fig.10 showed FCM histogram profiles of HeLa cells treated with different concentrations of MSNs-FITC at 50, 80 and 100  $\mu\text{g}\cdot\text{mL}^{-1}$ , respectively. Meanwhile, the FCM histogram profiles of HeLa cells showed quantitatively the changes of fluorescence intensity. It is clear that the fluorescence intensity increased obviously with increased concentrations of MSNs-FITC, which was consistent with the data of CLSM analysis, indicating effectively dose-depended internalization of MSNs-FITC.

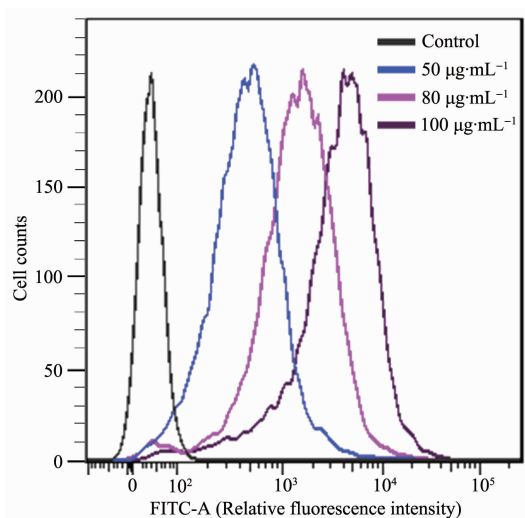


Fig.10 FCM histogram profiles of HeLa cells treated with different concentration of MSNs-FITC at 50, 80 and 100  $\mu\text{g}\cdot\text{mL}^{-1}$ , respectively

### 3 Conclusions

In summary, a drug delivery system mesoporous silica nanoparticles were prepared via a base-catalyzed sol-gel method. The well-defined nanoparticles were confirmed by the results from SEM, TEM, FTIR, BET, and UV-Vis spectra. DOX was applied as model drug to investigate drug loading and releasing behaviors. The nanoparticles possessed both high loading capacity (8.42%(w/w)) and encapsulation efficiency (65.7%). The cumulative release of DOX@MSNs-FITC showed a low leakage at pH value of 7.4 with only 38% amount being released after 24 h while significantly enhanced to 89% at pH value of 4.6. These results demonstrated that the drug release system was pH dependent apparently. The MTT cytotoxicity assay confirmed that the blank nanocarrier MSNs-FITC were almost non cytotoxicity on HeLa cells even at 100  $\mu\text{g}\cdot\text{mL}^{-1}$  after incubation for 24 h. CLSM analysis demonstrated that these can penetrate the plasma membrane of HeLa cells and transfer into the cytoplasm with high efficiency. FCM analysis indicated the internalization of nanocarriers was dose-depended. For further applications, the outermost surface of the MSNs-FITC should also be modified with pH-responsive ligands (e.g., polymer, supramolecular assemblies or inorganic nanoparticles) to enhance the

delivery efficiency and minimize adverse side effects.

### References:

- [1] Bray F, Ferlay J, Soerjomataram I, et al. *CA Cancer J. Clin.*, **2018**,**68**:394-424
- [2] Gao F P, Li L L, Fu C H, et al. *Adv. Mater.*, **2013**,**25**(38): 5508-5513
- [3] Chen X L, Sun H, Hu J, et al. *Colloids Surf. B*, **2017**,**152**: 77-84
- [4] Guo Y M, Li H, Shi W K, et al. *J. Colloid Interface Sci.*, **2017**,**502**:59-66
- [5] Zhang P F, Zhang L, Qin Z N, et al. *Adv. Mater.*, **2018**,**30** (7):1705350
- [6] Akhtar N, Khan R A. *Prog. Lipid Res.*, **2016**,**64**:192-230
- [7] Shen H J, Shi H, Ma K, et al. *Acta Biomater.*, **2013**,**9**(4): 6123-6133
- [8] Yang J Y, Kopeck J. *J. Drug Delivery Sci. Technol.*, **2015**, **30**(Part B):318-330
- [9] Sun H, She P, Lu G L, et al. *J. Mater. Sci.*, **2014**,**49**(20): 6845-6854
- [10] Li T T, Shi S X, Goel S, et al. *Acta Biomater.*, **2019**,**89**:1-13
- [11] Diab R, Canilho N, Pavel I A, et al. *Adv. Colloid Interface Sci.*, **2017**,**249**:346-362
- [12] Vallet-Regí M, Rámila A, del Real R P, et al. *Chem. Mater.*, **2001**,**13**(2):308-311
- [13] Hao N J, Jayawardana K W, Chen X, et al. *ACS Appl. Mater. Interfaces*, **2015**,**7**(2):1040-1045
- [14] Mai T B, Tran T N, Islam M R, et al. *J. Mater. Sci.*, **2014**, **49**(4):1519-1526
- [15] Tian Y, Glogowska A, Zhong W, et al. *J. Mater. Chem. B*, **2013**,**1**(39):5264-5272
- [16] Martínez C M, Lozano D, Colilla M, et al. *Acta Biomater.*, **2018**,**65**:393-404
- [17] Hu L L, Meng J, Zhang D D, et al. *Talanta*, **2018**,**177**:203-211
- [18] Steven C R, Busby G A, Mather C, et al. *J. Mater. Chem. B*, **2014**,**2**:5028-5042
- [19] Lee J E, Lee D J, Lee N, et al. *J. Mater. Chem.*, **2011**,**21**: 16869-16872
- [20] Kwon S, Singh R K, Kim T H, et al. *Acta Biomater.*, **2014**, **10**(3):1431-1442
- [21] Zhang Y, Hsu B Y W, Ren C L, et al. *Chem. Soc. Rev.*, **2015**,**44**(1):315-335
- [22] Yuan L, Tang Q Q, Yang D, et al. *J. Phys. Chem. C*, **2011**, **115**(20):9926-9932

- [23] Nguyen C T H, Webb R I, Lambert L K, et al. *ACS Appl. Mater. Interfaces*, **2017**,**9**(11):9470-9483
- [24] Begum G, Laxmi M V, Rana R K, et al. *J. Mater. Chem.*, **2012**,**22**:22174-22180
- [25] Zhang S L, Chu Z Q, Yin C, et al. *J. Am. Chem. Soc.*, **2013**, **135**(15):5709-5716
- [26] Hao W J, Shen Y X, Liu D Y, et al. *RSC Adv.*, **2017**,**7**:851-860
- [27] Narayan R, Nayak U Y, Raichur A M, et al. *Pharmaceutics*, **2018**,**10**:118
- [28] Wang J, Liu H Y, Leng F, et al. *Microporous Mesoporous Mater.*, **2014**,**186**(1):187-193
- [29] Hong C Y, Li X, Pan C Y. *J. Mater. Chem.*, **2009**,**19**(29): 5155-5160
- [30] Hu X X, Hao X H, Wu Y, et al. *J. Mater. Chem. B*, **2013**,**1**: 1109-1118
- [31] Jiao Y F, Guo J, Shen S, et al. *J. Mater. Chem.*, **2012**,**22** (34):17636-17643
- [32] Rim H P, Min K H, Lee H J, et al. *Angew. Chem. Int. Ed.*, **2011**,**50**(38):8853-8857
- [33] Chen Y Y, Ma P A, Yang D M, et al. *Chem. Asian J.*, **2014**, **9**(2):506-513
- [34] Gu J L, Su S S, Zhu M J, et al. *Microporous Mesoporous Mater.*, **2012**,**161**:160-167
- [35] Song G S, Li C, Hu J Q, et al. *J. Mater. Chem.*, **2012**,**22** (33):17011-17018
- [36] Mei X, Chen D Y, Li N J, et al. *Microporous Mesoporous Mater.*, **2012**,**152**:16-24
- [37] Popat A, Liu J, Lu G Q, et al. *J. Mater. Chem.*, **2012**,**22**: 11173-11178
- [38] Yu C M, Gao C M, Lü S Y, et al. *Colloids Surf. B*, **2014**, **115**:331-339
- [39] Zhao Z H, Huang D T, Yin Z Y, et al. *J. Mater. Chem.*, **2012**,**22**:15717-15725
- [40] Zhang Y Z, Wang J C, Bai X Y, et al. *Mol. Pharmaceutics*, **2012**,**9**(3):505-513